Journal of Biomechanics 85 (2019) 43–49

Contents lists available at ScienceDirect

Journal of Biomechanics

journal homepage: www.elsevier.com/locate/jbiomech
www.JBiomech.com

Numerical simulations of cell flow and trapping within microfluidic channels for stiffness based cell isolation

Mutabe S. Aljaghtham [a], Zixiang L. Liu [b], Jing J. Guo [c], Jin He [c], Emrah Celik [a,*]

[a] Department of Mechanical and Aerospace Engineering, University of Miami, USA
[b] Department Mechanical Engineering, Georgia Institute of Technology, USA
[c] Department of Physics, Florida International University, USA

ARTICLE INFO

Article history:
Accepted 3 January 2019

Keywords:
Stiffness
Deformation
Cell isolation
Finite element analysis
Cancer

ABSTRACT

Analysis of rare cells in heterogenous mixtures is proven to be beneficial for regenerative medicine, cancer treatment and prenatal diagnostics. Scarcity of these cells, however, makes the isolation process extremely challenging. Efficiency in cell isolation is still low and therefore, novel cell isolation strategies with new biomarkers need exploration. In this study, we investigated the feasibility of using the mechanical stiffness difference to detect and isolate the rare cells from the surrounding cells without labelling them. Fluid and solid mechanics simulations have shown that cell isolation can be performed at high efficiency using stiffness-based isolation. Accuracy of the numerical simulations is established using microfluidic flow chamber experiments.

1. Introduction

Isolating cells from heterogeneous mixtures is essential for many areas applications of biology, biotechnology, and medicine. Isolation and enrichment processes have become particularly important since the discovery of the diagnostic potential of rare cells such as circulating tumor cells (CTCs), hematopoietic stem cells (HSCs), and circulating fetal cells (CFCs) in blood (Shields et al., 2015). Analysis of CTCs in blood can be used to predict the metastatic potential, to monitor neoplastic progression and also to assess the primary tumor genetics (Khan et al., 2000). HSCs can differentiate into red blood cells, white blood cells and platelets and therefore HSCs possess utmost importance for regenerative medicine (Nakajima-Takagi et al., 2014). Similarly, circulating fetal cells carry genetic information of the fetus and hence these cells can be used for non-invasive prenatal diagnostics (Chen et al., 2014).

Although these rare cells possess unique therapeutic potential, detection and capture of these rare cells is a challenging procedure since their concentration in blood is extremely low. Immunomagnetic isolation is the most commonly used method to separate rare cells from the rest of the blood cells. In this technique, antibody against rare cell-specific biomarkers are attached to magnetic particles and mixed with medium containing rare cells. Magnetic beads bind to rare cells due to specific antibody-antigen interaction followed by separation via magnetic force. Immunomagnetic isolation is highly specific purification method and it lead to effective enrichment of rare cells in numerous studies (Jain et al., 2013; Krebs et al., 2014; Magbanua and Park, 2013; Stott et al., 2010; Yu et al., 2011). However, isolation efficacy in this method relies mainly on the expression level of the surface biomarkers/antigens on the cell membrane which has been reported to vary significantly (Gorges et al., 2012; Lara et al., 2004). In addition, the cost of antibodies conjugated to magnetic beads and the intensive labor required for the analysis of the test results are the drawbacks of immunomagnetic assays. Alternative to immunomagnetic separation is label-free isolation of rare cells based on the size difference. It has been reported previously that size of HSCs in bone marrow is larger than other present cells except of monocytes (Schirhagl et al., 2011). Similarly, size of certain tumor cells with epithelial origin (such as melanoma) is significantly larger than that of surrounding blood cells (Luo et al., 2014; Yu et al., 2011). Relative difference in rare cell size has been used to isolate these cells using microfluidic channels (Chen et al., 2016; Dong et al., 2013; Karabacak et al., 2014; Qi et al., 2012), parylene membrane filtration, (Zheng et al., 2007; Zheng et al., 2011), dielectrophoration (Gascoyne et al., 2009; Huang et al., 2013; Shim et al., 2013), and microchannel separation using centrifugal forces (Hou et al., 2013; Sollier et al., 2014; Warkiani et al., 2014, 2016). Isolation of rare cells based on the size variation is advantageous compared to the immunomagnetic separation due to its simplicity and the

* Corresponding author at: 1251 Memorial Drive, Coral Fables, FL 33146, USA.
E-mail address: e.celik@miami.edu (E. Celik).

https://doi.org/10.1016/j.jbiomech.2019.01.010
0021-9290/

high speed of the isolation process. However, most rare cells including HSCs and CTCs have comparable sizes to those of surrounding white blood cells (10–25 μm). As a result, white blood cells will inevitably be co-captured with the targeted rare cells in size based isolation leading to a low yield and purity.

We have recently showed that circulating tumor cells have additional distinctive property: mechanical stiffness or elastic modulus (Celik et al., 2015). The elastic modulus of melanoma cells (876 ± 127 Pa) is significantly lower than that of white blood cells (1962 ± 517 Pa). In addition, other documented, malignant cancer types such as breast, pancreatic and lung cancer cells have elastic moduli even lower than that of melanoma cells (Cross et al., 2007; Lekka and Laidler, 2009; Needham, 1991; Paszek et al., 2005; Xu et al., 2012) and therefore, these cancer cells possess higher potential to be isolated from blood cells using stiffness biomarker.

Recently, several studies investigated the potential of cell stiffness and deformability in cell isolation process. Shaw Bagnall et al. (2015) investigated time dependent deformability of single cells in suspended microchannel resonators (SMR). Preira et al. used microfluidic sieves in series with decreasing pore size in flow direction to sieve and trap cells based on size and deformability. (Preira et al., 2013). Similarly, Hur et al. adapted a microfluidic system to categorize cells by cell size and deformability to conduct label free cell enrichment using differences in dynamic equilibrium positions. The concept of slanted patterns within microfluidic chambers were introduced recently (Bongiorno et al., 2018; Islam et al., 2017; Islam et al., 2018; Wang et al., 2013) to deflect the cells from flow direction as a result of their deformability and separate the cells based on their stiffness. Most recently, Sajeesh et al. used stiffness contrast to isolate cells of different cell types from extremely stiff (E > 10 kPa) Hela cells (Sajeesh et al., 2016). The last two studies differ from the previous work on rare cell isolation since these studies use stiffness as the main parameter for cell separation. These studies showed that, cell stiffness can be an effective biomarker for such cell sorting applications.

The goal of this study is to develop a new, reliable, stiffness-based rare cell isolation platform which can be applicable to wide range of cell types without the need of high levels of differential stiffness between them. This requires quantitative investigation of cell deformation within microchannels and deciphering the relationship between cell size, cell stiffness and the channel geometry. In this study, solid and fluid mechanics simulations are used to investigate the parameters that effectively isolate rare cells in flow chambers. Solid mechanics simulations are performed to acquire the required hydrodynamic forces to capture or pass cells within a flow chamber. Fluid mechanics simulations are performed to determine how flow velocities are related to the hydrodynamic forces on cells. Quantitative analysis performed in this study allows precise control of fluid flow and separation of cells at high accuracy. The results of this analysis can be applied to microfluidics, as well as membrane filtering, for real time and high-throughput cell separation.

2. Materials and methods

2.1. Atomic force microscope (AFM) nanoindentation experiments

AFM nanoindentation experiments were performed to determine mechanical stiffness (modulus of elasticity) of cells. Details of the nanoindentation experiment is given in supplementary section S1. Experimentally acquired indentation and force data are then fitted into the Hertzian contact model as follows:

$$F = \frac{2E\tan(\alpha)}{\pi(1-\nu^2)}h^2 \quad (1)$$

In the equation above, α is the indenter angle, F is the contact force and h is indentation. We assumed the Poisson's ratio, ν to be 0.5 and the indenter angle, α as 55° according to the previously published work by Wojcikiewicz et al. (2004) We estimated Young's Modulus of Elasticity (E) by fitting Eq. (1) over experimental force and indentation data. Supplementary Fig. 1 shows the comparison between analytical model described above and the experimentally obtained force versus indentation response.

2.2. Fluid mechanics simulations

A 3-D CFD program based on the lattice-Boltzmann equation (LBE) method is developed to perform the fluid mechanics simulation and obtain the relationships between the inlet flow velocity and cell hydrodynamic force (see Fig. 1). As a kinetic-based mesoscopic approach, LBE method has been successfully applied to most of the low Reynolds number incompressible flow problems, particularly proven to be an ideal approach in dealing with particulate suspension flows due to its linear scalability and simplicity in parallelization (Aidun and Clausen, 2010; Chen and Doolen, 1998; Yu et al., 2003). More details concerning the LBE method are shown in the Supplementary Fig. 2.

2.3. Solid mechanics simulations

A parametric solid mechanics simulation study was performed to study the effect of cell size on the force to push the cells through the pores (pore diameter, D_{pore} = 10 μm) of a membrane.

Fig. 2 is a representative simulation of a passage of a cell with diameter of 13 μm. Initial approach, deformation and passage stages are shown in the figure. As shown in this figure, the pore with 10 μm size was kept constant and displacement boundary conditions were applied on the bottom boundary of the cell. As the cell is pulled down through the pore, force corresponding to each displacement amount was measured by summing all the reaction forces in the motion direction on the fixed boundary with the hole.

In order to quantify the effect of uncertainty in cell size in solid mechanics simulations, ±1 μm variation of cell size was considered. ANSYS simulations were performed according to the procedure described above and variation of cell passage force relative to the nominal value was quantified.

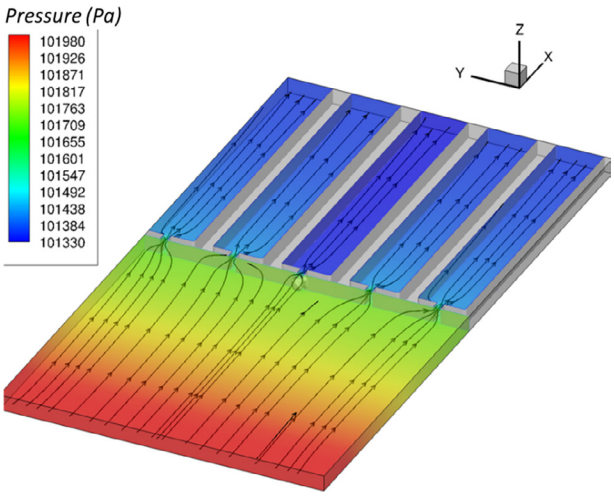

Fig. 1. Fluid mechanics simulation of a 18 μm cell trapped at the filter within a microfluidic chamber section.

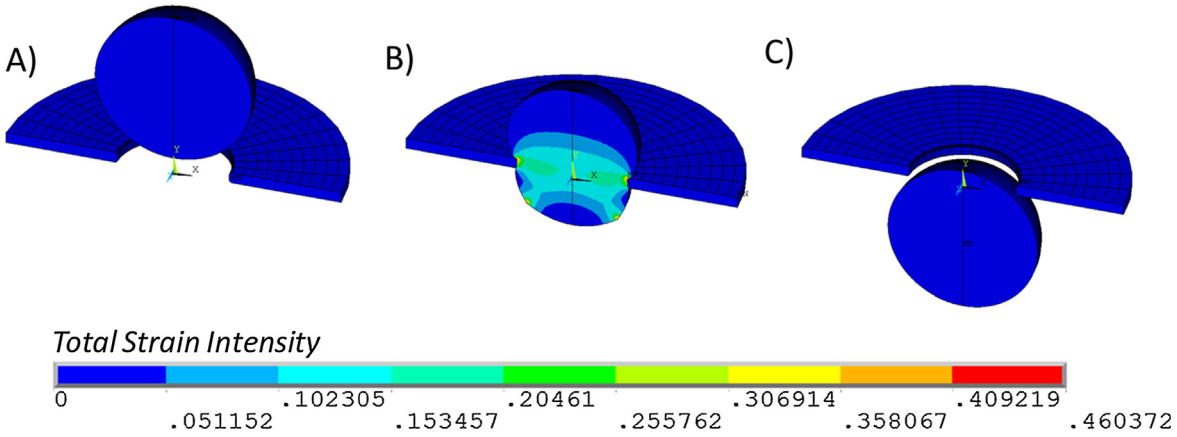

Fig. 2. Solid mechanics simulations of a 13 μm diameter cell passing a 10 μm pore. (A) Initial position, no-contact, (B) cell passage and deformation, (C) after the passage, no-contact.

2.4. Microfluidic chamber experiments

In order to test the validity of the fluid and solid mechanics simulations, we fabricated microfluidic based test chambers where we could trap individual cells and acquire critical fluid velocity values required to push the cells through the narrow channel openings. A finished product is shown in Fig. 3 below. Fig. 3A represents the macroscopic view of the fabricated test chamber with multi channels. Fig. 3B shows the details of one channel, which contains multiple narrow openings for cell passage. The width of an opening is 10 μm and the height of the flow chamber is 25 μm.

For the cell trapping experiments, we run MCF-7 cell solution in the microfluidic chambers until a large cell is trapped at a channel. The flow rate is then gradually increased until the trapped cell passes the channel. This passing velocity represents the critical velocity observed experimentally. Since cells can show viscoelastic behaviour, we waited 2 min before each flow rate increment to minimize the effects of time dependent deformation.

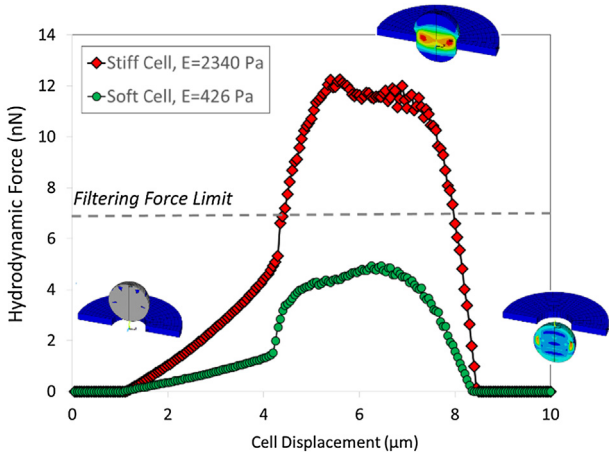

Fig. 4. Variation of contact force on stiff and soft cells as a function of cell displacement.

3. Results

3.1. Isolation of soft and stiff cells based on stiffness difference

Isolation of soft and stiff cells with different elastic modulus properties are simulated via finite element analysis. Fig. 4 represents how contact force changes during passage of soft (tumor) and stiff cells through a membrane pore. Both cells have the same cell sizes (13 μm) but different stiffness/modulus values. Numerical simulation starts when there is no contact between the cell and the membrane (net force on the cell is zero) and the cell moves toward the pore of the membrane at a constant velocity. As the cell comes into contact with the pore of the membrane filter, contact force starts increasing until the critical contact force is achieved. As the cell continues to deform and passes through the filter, con-

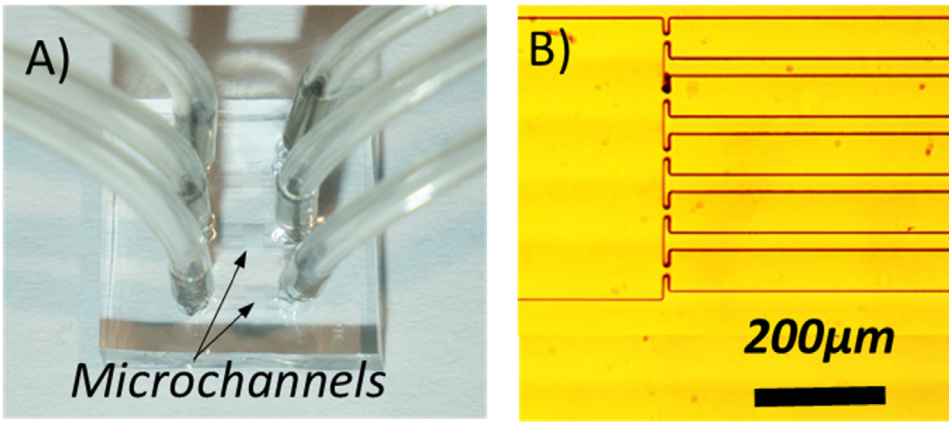

Fig. 3. (A) Image of a fabricated device with multi test channels. (B) An optical microscope image to show the details of a channel with five narrow openings.

tact force drops back to the initial zero value as shown in Fig. 4. If the force applied on the cell exceeds the critical contact force (maximum force) as shown in Fig. 4, the cell will pass the filter, otherwise cell will stay attached to the pore of the membrane and captured. Therefore, hydrodynamic force exerted on the cells (dashed line in Fig. 4) can be used to separate the soft cells from the stiff ones. In other words, about 12 nN force is required to push the stiff cell through the membrane pore. In contrast, only 4 nN is needed for the soft cell. Hence, if a maximum force of 7 nN is applied on these cells, soft cell will pass the pore but the stiff one will be captured by the membrane; since the applied force does not exceed the critical contact force for the stiff cell (12 nN). Therefore, soft and stiff cells can be separated with high efficiency based on their stiffness only assuming that all cells have similar sizes.

In order to quantify synergistic effects of cell size and cell stiffness on the critical force, cell passage was simulated by varying soft and stiff cell sizes within the range of 12–14 μm. Fig. 5 below shows the required critical force level for cell passage of each cell type. As shown in the figure, if 10 nN force is applied for size separation, any cell in the red zone cannot pass the membrane filter since critical force for these cells are not achieved. Cells located in the green zone passes the pore and separated from those in the red zone. It is clear from the figure that, under these conditions, all stiff cells are captured by the membrane filter and almost all soft cells passes in the considered size range (12–14 μm) except those within 13.8–14 μm. These new results show that cells can be isolated very effectively even cell variation of ±1 μm is considered. However, efficiency will reduce significantly for higher cell size variations and it must be minimized to achieve the highest possible cell isolation using the described stiffness-based isolation methodology.

3.2. Hydrodynamic force vs inlet velocity

In the actual cell isolation process, hydrodynamic force acting on a cell cannot be a control parameter. Instead, the flow velocity can be adjusted and the pressure field and consequently, force exerted on the trapped cells can be altered. Therefore, it is essential to assess the relationship between hydrodynamic force on a trapped cell versus inlet flow velocity for practical cell isolation applications. As a first step for this assessment, we determined the pressure field corresponding to different inlet flow velocities. Fig. 6 below shows the pressure field across an individual cell trapped by a membrane pore. As the velocity is increased, pressure level and therefore force on the cell increased. Fig. 6A–C correspond to the pressure fields for the inlet velocity of 0.94 mm/s, 2.36 mm/s and 4.71 mm/s respectively.

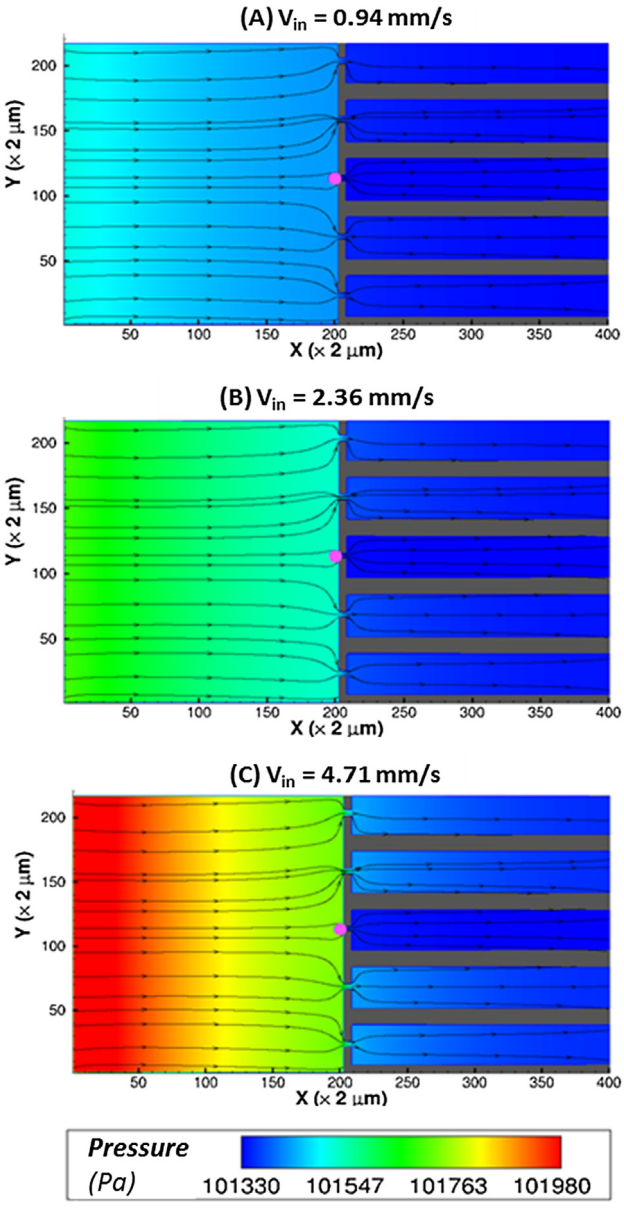

Fig. 6. Pressure variation for the case of single 16 μm cell being trapped by the filter when different inlet velocity (A) 0.94 mm/s, (B) 2.36 mm/s and (C) 4.71 mm/s being applied.

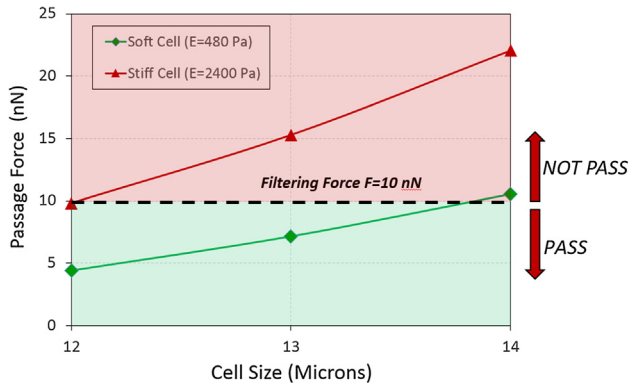

Fig. 5. Variation of critical (maximum) force on stiff and soft cells as a function of cell size.

Hydrodynamic forces corresponding to flow pressures acting on cells along channel length (x-direction) are calculated by multiplying cell surface area and the flow pressure. Calculated hydrodynamic forces are plotted in Fig. 7 for 5 different cell sizes (12 μm, 14 μm, 16 μm, 18 μm and 20 μm). Variation of hydrodynamic force was found to be linear as a function of flow velocity and force increases rapidly as the cell size is increased.

Fluid mechanics simulation results shown in Figs. 6 and 7 along with solid mechanics results given in Fig. 4 allow us to determine the critical velocity required to pass a cell through a pore. Only parameters affecting this passage velocity are the size and stiffness of the cell. By using this information, cells of similar sizes can be separated using the mechanical stiffness parameter and by simply controlling the velocity of the fluid flow in microfluidic chambers.

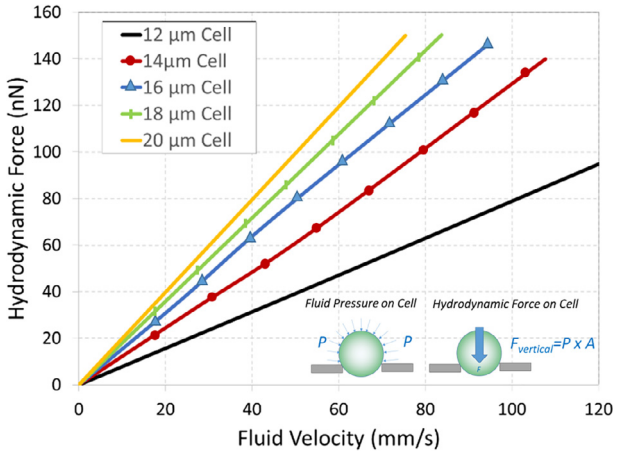

Fig. 7. Hydrodynamic force varies with different inlet velocity for trapped cells of different sizes (12–20 μm).

3.3. Validation of cell isolation models via microfluidic experiments

Microfluidic flow chamber experiments were used to validate the simulation results. MCF-7 cells were trapped within the channels of the fabricated microfluidic device and the experimentally observed critical velocity required to pass the cells through the channels were compared to those obtained from the numerical simulations. Critical velocity, or velocity required to push a cell toward a channel is an ideal parameter to validate the numerical simulations since this parameter can easily be obtained from microfluidic experiments and numerical simulations. Experimentally, we obtained the passing velocity on a trapped cell by gradually increasing the velocity until the cell passes the channel. The minimum velocity which is sufficient to push the cell through the channel is the critical passing velocity. Fig. 8A shows a representative cell (with a diameter of 18 μm) trapped over the channel opening at low flow velocity. As the flow velocity is increased, force on the cell and therefore cell deformation increased (Fig. 8B and C). The cell finally passed the opening when the flow rate exceeded the critical velocity. Critical flow velocity was obtained by simply dividing volumetric flow rate by microfluidic channel area.

Numerically, we can acquire this parameter by first simulating structural analysis of a cell passing a membrane opening and finding the maximum force required to balance the resistance exerted on the cell by the channel. The channel resistance is correlated to the stiffness or elastic modulus of the trapped cell. Elastic modulus of MCF-7 cells were measured to be 1127.8 ± 176.6 Pa and shown in Supplementary Fig. 3. The modulus of MCF-7 is comparable to the published literature data for these cell type (Dokukin et al., 2013; Lee et al., 2012). After structural analysis, we simulated the fluid flow around a trapped cell, and determined the critical velocity required to apply the passing force calculated in the previous step.

Fig. 9 shows the comparison of numerical predictions versus experimental values for the critical velocities. Variation of hydrodynamic force versus velocity plots for the cell size of 18 μm and 20 μm are given by red and green colors. According to these plots, if the force (and velocity) level is in red line region, critical force is not achieved and the cell is trapped in the pore opening. Otherwise, force is sufficient to push the cell across the opening and the cell passes the pore. Therefore, the critical forces and velocities are predicted to be at the junctions of red and green colors acquired by numerical simulations.

Computational simulations discussed above predict the critical velocities for the passage of 18 μm cell as 44.8 mm/s and 20 μm cell as 63.3 mm/s. Experimentally obtained critical velocities for 18 μm and 20 μm cells are 52.2 mm/s and 63.4 mm/s, respectively. Therefore, error between experiments and the numerical simulations is less than 15 percent and our simulations can represent the actual events taking place within the flow chambers.

4. Conclusions and discussion

Isolating rare cells from the cell mixtures is a challenging process due to the scarcity of these cells in the mixture medium. Mechanical stiffness biomarker offers a new isolation process based on different stiffness between rare cells and their surroundings. This study is a novel attempt to quantitatively determine the relationships between biophysical properties of cells and the control parameters of the cell filtration process. Solid and fluid mechanics simulations are used to establish the relationship between cell size, cell stiffness and channel opening to trap cells based on their stiffness properties.

Fluid mechanics simulations used in this study can capture the fluid velocity and the force acting on cells trapped within a membrane opening. Solid mechanics simulations can then determine if this force is sufficiently high to deform the cell and pass the membrane. For stiffer cells (such as white blood cells) higher levels of

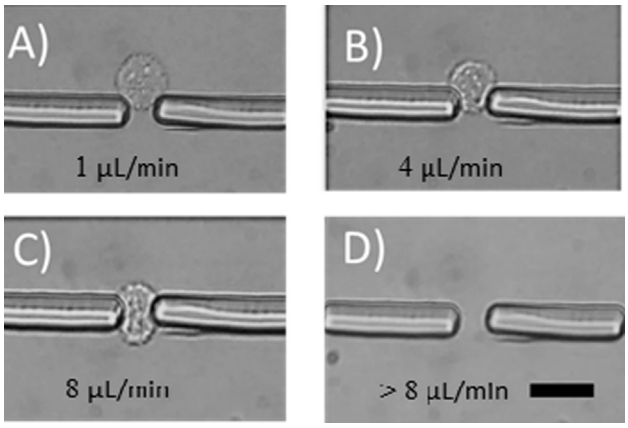

Fig. 8. Cell deformation versus flow rate within the microfluidic chamber. (A) Cell is trapped at low flow rate. (B) Flow rate is increased and cell deformation starts (C) Flow rate is equal to critical velocity (D) Cell passes the pore at velocity higher than the critical velocity. Scale bar represent the length of 20 μm.

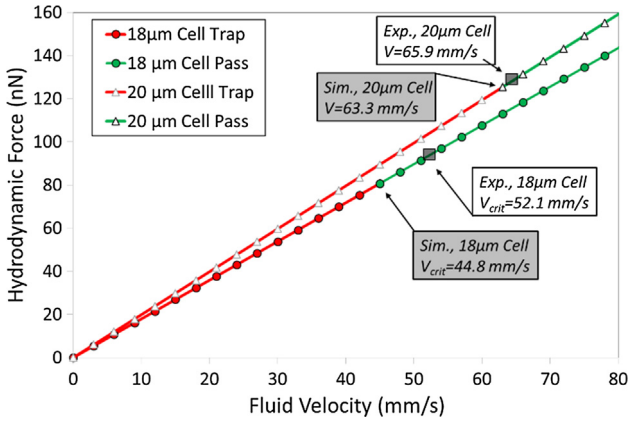

Fig. 9. Comparison of critical velocity predictions via solid-fluid mechanics simulations and experimental observations for 2 cell sizes. Red regions shows the force/velocity levels of trapping, green regions shows the level of passing. (For interpretation of the references to colour in this figure legend, the reader is referred to the web version of this article.)

force is required compared to softer cells (such as cancer cells). Therefore, if a force level which is between critical forces of soft and stiff cells is applied on the solution involving these cells, soft cells will pass the pores of the membrane and stiff cells will be trapped. Hence, cell mixtures will be separated by solely stiffness of these cells.

Using the results obtained in this study, high throughput cell sorting and isolation systems can be designed and developed. A feasible concept of stiffness based isolation platform is shown in Fig. 10A below. In this device, cells are flown within the filtration chamber by the syringe pump and trapped by the filter which has smaller pore size compared to size of cells. If sufficient force/-pressure is applied on cells by the pump, cells will deform and pass the filter. The amount of force to be applied on the cells is directly correlated to the stiffness or elastic modulus of the cells.

Although flow velocity is a simple parameter to control fluid flow, in the actual membrane filtration experiment, stiff cells will gradually be trapped within pores of the filtration membrane. If the flow velocity is kept constant, pressure and therefore force on the trapped cells will increase due to membrane clogging and increased pressure will lead to passing of stiff cells along soft ones as well. In order to keep the force and pressure steady on these cells, a pressure sensor must be used in the filtration system.

As the pores of the membrane filter are clogged, the flow velocity will decrease to keep the pressure constant. Commercially available, 25 mm diameter, tracked etched filters possess 10–100 millions of pores. If the cell mixture has comparable or higher amount of cells than the number of pores, filter clogging and replacement may be required. If this is the case, flow valve can be closed to stop the flow, membrane is taken out, replaced with a new one and the flow is restarted as shown in Fig. 10B.

Another challenge of the stiffness filtration process might be observed when isolating cells with different sizes. This study assumes that isolated cells have similar diameters. However, in cell mixtures, size variation is expected for even same type of cells. In order to reduce size difference and use stiffness as the only isolation biomarker, initial size sorting must be performed. Current cell sorting methods offer excellent cell size sorting within <2 μm resolution. We believe that <1 μm resolution should be possible in near future which will significantly enhance efficiency of stiffness based isolation method described in this study.

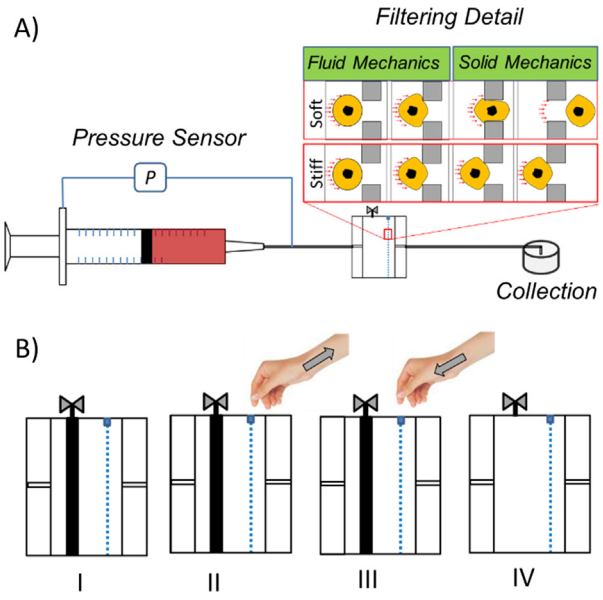

Fig. 10. (A) Schematic of the stiffness-based isolation platform, (B) Steps of a simple filter replacement process (I: Close the flow valve, II: Take out the clogged filter, III: Replace a new filter, IV: Open the flow valve).

Acknowledgements

This work was supported by the UM and FIU start-up funds, UM Provost Award and NSF (CMMI1334417) grant. We also would like to thank Kadir Ozkan from Stoneline Group, LLC for his help with the construction of the AFM.

Conflict of interest

All of the authors of this study certify that they have no affiliations with or involvement in any organization or entity with any financial or non-financial interest in the subject matter or material.

Appendix A. Supplementary material

Supplementary data to this article can be found online at https://doi.org/10.1016/j.jbiomech.2019.01.010.

References

Aidun, C.K., Clausen, J.R., 2010. Lattice-Boltzmann method for complex flows. Annu. Rev. Fluid Mech. 42, 439–472.
Bongiorno, T., Gura, J., Talwar, P., Chambers, D., Young, K.M., Arafat, D., Wang, G., Jackson-Holmes, E.L., Qiu, P., McDevitt, T.C., et al., 2018. Biophysical subsets of embryonic stem cells display distinct phenotypic and morphological signatures. PLoS ONE 13, (3) e0192631.
Celik, E.R.N., Bahamonde, A., Ao, Z., Datar, R., 2015. Isolation of Circulating Tumor Cells Using Stiffness Based Filtration Platform. IMECE2015. Houston, TX.
Chen, J.Y., Tsai, W.S., Shao, H.J., Wu, J.C., Lai, J.M., Lu, S.H., Hung, T.F., Yang, C.T., Wu, L.C., Chen, J.S., et al., 2016. Sensitive and specific biomimetic lipid coated microfluidics to isolate viable circulating tumor cells and microemboli for cancer detection. PLoS ONE 11 (3).
Chen, S., Doolen, G.D., 1998. Lattice Boltzmann method for fluid flows. Annu. Rev. Fluid Mech. 30, 329–364.
Chen, Y., Li, P., Huang, P.H., Xie, Y., Mai, J.D., Wang, L., Nguyen, N.T., Huang, T.J., 2014. Rare cell isolation and analysis in microfluidics. Lab Chip 14 (4), 626–645.
Cross, S.E., Jin, Y.S., Rao, J., Gimzewski, J.K., 2007. Nanomechanical analysis of cells from cancer patients. Nat. Nanotechnol. 2 (12), 780–783.
Dokukin, M.E., Guz, N.V., Sokolov, I., 2013. Quantitative study of the elastic modulus of loosely attached cells in AFM indentation experiments. Biophys. J. 104 (10), 2123–2131.
Dong, Y., Skelley, A.M., Merdek, K.D., Sprott, K.M., Jiang, C.S., Pierceall, W.E., Lin, J., Stocum, M., Carney, W.P., Smirnov, D.A., 2013. Microfluidics and circulating tumor cells. J. Mol. Diagn. 15 (2), 149–157.
Gascoyne, P.R., Noshari, J., Anderson, T.J., Becker, F.F., 2009. Isolation of rare cells from cell mixtures by dielectrophoresis. Electrophoresis 30 (8), 1388–1398.
Gorges, T.M., Tinhofer, I., Drosch, M., Rose, L., Zollner, T.M., Krahn, T., von Ahsen, O., 2012. Circulating tumour cells escape from EpCAM-based detection due to epithelial-to-mesenchymal transition. Bmc Cancer 12.
Hou, H.W., Warkiani, M.E., Khoo, B.L., Li, Z.R., Soo, R.A., Tan, D.S.W., Lim, W.T., Han, J., Bhagat, A.A.S., Lim, C.T., 2013. Isolation and retrieval of circulating tumor cells using centrifugal forces. Sci. Rep.-UK, 3.
Huang, S.B., Wu, M.H., Lin, Y.H., Hsieh, C.H., Yang, C.L., Lin, H.C., Tseng, C.P., Lee, G.B., 2013. High-purity and label-free isolation of circulating tumor cells (CTCs) in a microfluidic platform by using optically-induced-dielectrophoretic (ODEP) force. Lab Chip 13 (7), 1371–1383.
Islam, M., Brink, H., Blanche, S., DiPrete, C., Bongiorno, T., Stone, N., Liu, A., Philip, A., Wang, G., Lam, W., et al., 2017. Microfluidic sorting of cells by viability based on differences in cell stiffness. Sci. Rep. 7 (1), 1997.
Islam, M., Mezencev, R., McFarland, B., Brink, H., Campbell, B., Tasadduq, B., Waller, E.K., Lam, W., Alexeev, A., Sulchek, T., 2018. Microfluidic cell sorting by stiffness to examine heterogenic responses of cancer cells to chemotherapy. Cell Death Dis. 9 (2), 239.
Jain, J., Veggiani, G., Howarth, M., 2013. Cholesterol loading and ultrastable protein interactions determine the level of tumor marker required for optimal isolation of cancer cells. Cancer Res. 73 (7), 2310–2321.
Karabacak, N.M., Spuhler, P.S., Fachin, F., Lim, E.J., Pai, V., Ozkumur, E., Martel, J.M., Kojic, N., Smith, K., Chen, P.I., et al., 2014. Microfluidic, marker-free isolation of circulating tumor cells from blood samples. Nat. Protoc. 9 (3), 694–710.
Khan, Z.A., Jonas, S.K., Le-Marer, N., Patel, H., Wharton, R.Q., Tarragona, A., Ivison, A., Allen-Mersh, T.G., 2000. P53 mutations in primary and metastatic tumors and circulating tumor cells from colorectal carcinoma patients. Clin. Cancer Res.: An Off. J. Am. Assoc. Cancer Res. 6 (9), 3499–3504.

Krebs, M.G., Metcalf, R.L., Carter, L., Brady, G., Blackhall, F.H., Dive, C., 2014. Molecular analysis of circulating tumour cells-biology and biomarkers. Nat. Rev. Clin. Oncol. 11 (3), 129–144.

Lara, O., Tong, X., Zborowski, M., Chalmers, J.J., 2004. Enrichment of rare cancer cells through depletion of normal cells using density and flow-through, immunomagnetic cell separation. Exp. Hematol. 32 (10), 891–904.

Lee, M.H., Wu, P.H., Staunton, J.R., Ros, R., Longmore, G.D., Wirtz, D., 2012. Mismatch in mechanical and adhesive properties induces pulsating cancer cell migration in epithelial monolayer. Biophys. J. 102 (12), 2731–2741.

Lekka, M., Laidler, P., 2009. Applicability of AFM in cancer detection. Nat. Nanotechnol. 4 (2). 72-72.

Luo, X,, Mitra, D., Sullivan, R.J., Wittner, B.S., Kimura, A.M., Pan, S.W., Hoang, M.P., Brannigan, B.W., Lawrence, D.P., Flaherty, K.T., et al., 2014. Isolation and molecular characterization of circulating melanoma cells. Cancer Res., vol. 74, 19.

Magbanua, M.J.M., Park, J.W., 2013. Isolation of circulating tumor cells by immunomagnetic enrichment and fluorescence-activated cell sorting (IE/FACS) for molecular profiling. Methods 64 (2), 114–118.

Nakajima-Takagi, Y., Osawa, M., Iwama, A., 2014. Manipulation of hematopoietic stem cells for regenerative medicine. Anat. Rec. 297 (1), 111–120.

Needham, D., 1991. Possible role of cell cycle-dependent morphology, geometry, and mechanical-properties in tumor-cell metastasis. Cell Biophys. 18 (2), 99–121.

Paszek, M.J., Zahir, N., Johnson, K.R., Lakins, J.N., Rozenberg, G.I., Gefen, A., Reinhart-King, C.A., Margulies, S.S., Dembo, M., Boettiger, D., et al., 2005. Tensional homeostasis and the malignant phenotype. Cancer Cell 8 (3), 241–254.

Preira, P., Grandne, V., Forel, J.M., Gabriele, S., Camara, M., Theodoly, O., 2013. Passive circulating cell sorting by deformability using a microfluidic gradual filter. Lab Chip 13 (1), 161–170.

Qi, D., Hoelzle, D.J., Rowat, A.C., 2012. Probing single cells using flow in microfluidic devices. Eur. Phys. J.-Spec Top. 204 (1), 85–101.

Sajeesh, P., Raj, A., Doble, M., Sen, A.K., 2016. Characterization and sorting of cells based on stiffness contrast in a microfluidic channel. Rsc Adv. 6 (78), 74704–74714.

Schirhagl, R., Fuereder, I., Hall, E.W., Medeiros, B.C., Zare, R.N., 2011. Microfluidic purification and analysis of hematopoietic stem cells from bone marrow. Lab Chip 11 (18), 3130–3135.

Shaw Bagnall, J., Byun, S., Begum, S., Miyamoto, D.T., Hecht, V.C., Maheswaran, S., Stott, S.L., Toner, M., Hynes, R.O., Manalis, S.R., 2015. Deformability of tumor cells versus blood cells. Sci. Rep. 5, 18542.

Shields, C.W., Reyes, C.D., Lopez, G.P., 2015. Microfluidic cell sorting: a review of the advances in the separation of cells from debulking to rare cell isolation. Lab Chip 15 (5), 1230–1249.

Shim, S., Stemke-Hale, K., Tsimberidou, A.M., Noshari, J., Anderson, T.E., Gascoyne, P. R.C., 2013. Antibody-independent isolation of circulating tumor cells by continuous-flow dielectrophoresis. Biomicrofluidics 7 (1).

Sollier, E., Go, D.E., Che, J., Gossett, D.R., O'Byrne, S., Weaver, W.M., Kummer, N., Rettig, M., Goldman, J., Nickols, N., et al., 2014. Size-selective collection of circulating tumor cells using Vortex technology. Lab Chip 14 (1), 63–77.

Stott, S.L., Lee, R.J., Nagrath, S., Yu, M., Miyamoto, D.T., Ulkus, L., Inserra, E.J., Ulman, M., Springer, S., Nakamura, Z., et al., 2010. Isolation and characterization of circulating tumor cells from patients with localized and metastatic prostate cancer. Sci. Transl. Med. 2 (25), 25ra23.

Wang, G.H., Mao, W.B., Byler, R., Patel, K., Henegar, C., Alexeev, A., Sulchek, T., 2013. Stiffness dependent separation of cells in a microfluidic device. PLoS ONE 8 (10).

Warkiani, M.E., Guan, G.F., Luan, K.B., Lee, W.C., Bhagat, A.A.S., Chaudhuri, P.K., Tan, D.S.W., Lim, W.T., Lee, S.C., Chen, P.C.Y., et al., 2014. Slanted spiral microfluidics for the ultra-fast, label-free isolation of circulating tumor cells. Lab Chip 14 (1), 128–137.

Warkiani, M.E., Khoo, B.L., Wu, L.D., Tay, A.K.P., Bhagat, A.A.S., Han, J., Lim, C.T., 2016. Ultra-fast, label-free isolation of circulating tumor cells from blood using spiral microfluidics. Nat. Protoc. 11 (1), 134–148.

Wojcikiewicz, E.P., Zhang, X., Moy, V.T., 2004. Force and compliance measurements on living cells using atomic force microscopy (AFM). Biol. Proc. Online 6, 1–9.

Xu, W.W., Mezencev, R., Kim, B., Wang, L.J., McDonald, J., Sulchek, T., 2012. Cell stiffness is a biomarker of the metastatic potential of ovarian cancer cells. PLoS ONE 7 (10).

Yu, D.Z., Mei, R.W., Luo, L.S., Shyy, W., 2003. Viscous flow computations with the method of lattice Boltzmann equation. Prog. Aerosp. Sci. 39 (5), 329–367.

Yu, M., Stott, S., Toner, M., Maheswaran, S., Haber, D.A., 2011. Circulating tumor cells: approaches to isolation and characterization. J. Cell Biol. 192 (3), 373–382.

Zheng, S., Lin, H., Liu, J.Q., Balic, M., Datar, R., Cote, R.J., Tai, Y.C., 2007. Membrane microfilter device for selective capture, electrolysis and genomic analysis of human circulating tumor cells. J. Chromatogr. A 1162 (2), 154–161.

Zheng, S., Lin, H.K., Lu, B., Williams, A., Datar, R., Cote, R.J., Tai, Y.C., 2011. 3D microfilter device for viable circulating tumor cell (CTC) enrichment from blood. Biomed. Microdev. 13 (1), 203–213.